HTML ABSTRACT + LINKS

JOURNAL OF CHEMICAL PHYSICS VOLUME 121, NUMBER 17 1 NOVEMBER 2004

The mechanism of proton exchange: Guided ion beam studies of the reactions, $H(H_2O)_n^+$ ($n=1-4$)+D_2O and $D(D_2O)_n^+$ ($n=1-4$)+H_2O

Kenji Honma
Department of Material Science, University of Hyogo, Kamigori, Hyogo, 678-1297 Japan

P. B. Armentrout
Department of Chemistry, University of Utah, Salt Lake City, Utah 84112

(Received 29 July 2004; accepted 11 August 2004)

Reactions of protonated water clusters, $H(H_2O)_n^+$ ($n=1-4$) with D_2O and their "mirror" reactions, $D(D_2O)_n^+$ ($n=1-4$) with H_2O, are studied using guided-ion beam mass spectrometry. Absolute reaction cross sections are determined as a function of collision energy from thermal energy to over 10 eV. At low collision energies, we observe reactions in which H_2O and D_2O molecules are interchanged and reactions where H-D exchange has occurred. As the collision energy is increased, the H-D exchange products decrease and the water exchange products become dominant. At high collision energies, processes in which one or more water molecules are lost from the reactant ions become important, with simple collision-induced dissociation processes, i.e., those without H-D exchange, being dominant. Threshold energies of endothermic channels are measured and used to determine binding energies of the proton bound complexes, which are consistent with those determined by thermal equilibrium measurements and previous collision-induced dissociation studies. A kinetic scheme that relies only on the ratio of isomerization and dissociation rate constants successfully accounts for the kinetic energy dependence observed in the branching ratios for H-D and water exchange products in all systems. Rice–Ramsperger–Kassel–Marcus theory and *ab initio* calculations confirm the feasibility and establish the details of this kinetic model. © *2004 American Institute of Physics.* [DOI: 10.1063/1.1802391]

I. INTRODUCTION

One of the best studied proton transfer reactions is the symmetric exchange between water molecules.[1–7] Of necessity, this requires isotopic labeling studies such that either the $H_3O^+ + D_2O$ or the $D_3O^+ + H_2O$ reaction has been examined. An added point of interest in such systems is that there are two channels now available, simple proton (or deuteron) transfer to form $HD_2O^+ + H_2O$ ($H_2DO^+ + D_2O$) and the isotope scrambling reaction to yield $H_2DO^+ + HDO$ ($HD_2O^+ + HDO$). As discussed in more detail below, the former process can occur readily in reactions proceeding by both direct and complex formation, whereas the latter requires an intermediate that lives at least for vibrational periods in order to permit the rearrangement required. Indeed, in a crossed-beam study of this process, Ryan *et al.* find that both channels are observed at a collision energy of 0.7 eV, whereas only simple proton transfer is observed between 2 and 5 eV.[1] However, they find that the mechanism for both processes is identical and there is no evidence for an abrupt change from a complex mechanism at low energies to a direct mechanism at high energies. This is consistent with a recent theoretical study by Bowman's group, which suggests that the intermediate complex for the reaction $H_3O^+ + H_2O$ is long lived even at fairly high collision energies.[2]

The most thorough studies of this reaction have been conducted by Adams, Smith, and Henchman under thermal conditions in a flow tube at both 295 and 495 K.[3,4] Here, isotope scrambling is essentially complete with a 30:70 (35:65) distribution of HD_2O^+:H_2DO^+ (H_2DO^+:HD_2O^+) ionic products. In the absence of isotope effects, the statistical result is 33:67 for both reactions. The small deviations from this prediction can be attributed to differences in zero-point energies, which favor the less deuterated ionic species in both reaction system.[5] Recent ion cyclotron resonance (ICR) mass spectrometry results of Anicich and Sen do not confirm these results, obtaining instead a less completely equilibrated distribution.[7]

Henchman, Smith, and Adams[6] go on to propose a kinetic model for the competition between these two reactions that relies on a single parameter κ, which equals the rate of isomerization k_j, divided by the rate of dissociation k_d. Although the results of this model reproduce the limited thermal data, the model is incorrectly based on a two-well potential energy surface for the $H_3O^+ \cdot D_2O$ complex, i.e., $H_3O^+ \cdot D_2O$ and $H_2O \cdot HD_2O^+$ are taken to be distinct intermediates that dissociate exclusively to $H_3O^+ + D_2O$ and $HD_2O^+ + H_2O$, respectively. Oddly, in previous papers,[5] the same authors correctly state that this system is governed by a deep single-well potential $H_2O \cdot H^+ \cdot D_2O$,[8,9] which can dissociate either to $H_3O^+ + D_2O$ or $HD_2O^+ + H_2O$. Nevertheless, the concepts introduced in this kinetic treatment are correct even if the application is flawed in detail. Hence, we rederive the kinetic model in the present work using the correct chemistry and utilize *ab initio* calculations and Rice–Ramsperger–Kassel–Marcus (RRKM) statistical theory to demonstrate its feasibility.

 © 2004 American Institute of Physics

Downloaded 11 Aug 2009 to 155.97.13.46. Redistribution subject to AIP license or copyright; see http://jcp.aip.org/jcp/copyright.jsp

One of the predictions made in this kinetic model is how the branching ratio and overall reaction efficiency η changes as κ is varied. It would be nice to find a means to experimentally vary this quantity. In thinking about this (significantly, in retrospect rather than prior to our experiments), we realized that the kinetic energy dependence of k_j and k_d should differ because the former reaction must involve a tight transition state, whereas the latter evolves over a loose (orbiting) transition state. Further, the activation energies for the isomerization and dissociation steps must differ. The activation energy for dissociation is known and equals the binding energy of the $H_3O^+ \cdot H_2O$ complex, 140 kJ/mol.[10–14] Clearly, the activation energy for isomerization must be less than this otherwise complete scrambling of the isotopic labels would not occur for collisions of the $H_3O^+ + D_2O$ reactants at thermal energies. This is also obvious from the qualitative branching ratios obtained in the crossed-beam study. Therefore, examination of the kinetic energy dependence of the $H_3O^+ + D_2O$ reaction and its mirror $D_3O^+ + H_2O$ provides quantitative insight into the relative rates of isomerization and dissociation.

In addition to examination of this simple proton transfer and complex isomerization reaction, we are also interested in how solvation of the proton affects the rates of these reactions. Solvation effects on chemistry are fundamental to the kinetics and thermodynamics of all condensed phase systems. By studying changes in reactivity induced by stepwise addition of solvent molecules to the system under examination, we can help to bridge the gap between the gas phase and the solution phase.[15–18] Smith, Adams, and Henchman[4] have used the SIFT (selected ion flow tube) technique to examine the reactions of $H(H_2O)_n^+$ clusters with D_2O for $n = 1-3$. Their results show that the thermal rate constants are $1.7-2.2\times 10^{-9}$ cm^3 s^{-1} and are not sensitive to the cluster size nor isotopic substitution. With respect to reactions in which H-D atoms are exchanged, Smith *et al.*[4] observed that the distribution of H and D amongst the product ions was almost statistical up to $n=2$ cluster ions.

Previously, we determined the kinetic energy dependence of the cross sections for reaction of protonated water clusters $H(H_2O)_n^+$ ($n=1-4$) with deuterated ammonia ND_3 and acetonitrile CH_3CN, using a guided-ion beam apparatus.[15,16] (The formulas $H(H_2O)_n^+$ are used throughout this paper primarily as a book-keeping measure because the reactions are dominated by transfer and loss of intact water molecules. These formulas do not accurately represent the structures of these ions.) Total reaction rates are rather insensitive to the cluster size, and the dominant reaction products at thermal energies in both cases are solvent exchanged cluster ions, $H(ND_3)(H_2O)_{n-2}^+$ and $H(CH_3CN)(H_2O)_{n-1}^+$, where the former reaction is more exothermic thereby leading to more extensive dissociation. At higher collision energies, these species dissociate to form smaller proton bound clusters. The results are consistent with a mechanism that forms an intermediate complex, probably involving hydrogen bonding between $H(H_2O)_n^+$ and ND_3 (or CH_3CN),[19] which decomposes by loss of H_2O or ND_3 (CH_3CN) (Ref. 20) as its internal energy increases. In the reactions with ND_3, we found no products in which H-D exchange had occurred. This result implies that H_2O and ND_3 can be treated as integral units and the lifetime of the intermediate complex is not long enough for H-D exchange between H_2O and ND_3 molecules.

In this work, we extend our studies of solvation to the reactions of $H(H_2O)_n^+$ with D_2O and their "mirror" reactions, $D(D_2O)_n^+$ with H_2O, where $n=1-4$. These systems are also characterized by the presence of potential minima that correspond to hydrogen bonded intermediates, $H(H_2O)_n(D_2O)^+$ or $D(D_2O)_n(H_2O)^+$.[10–14] In contrast to the ND_3 and CH_3CN systems where the proton transfer reactions are strongly exothermic, proton exchange between H_2O and D_2O units is nearly thermoneutral because both molecules are chemically equivalent. Thus, the reactions are long lived allowing extensive isomerization and hydrogen migration and thereby provide a unique opportunity to study such processes without strong thermodynamic driving forces.

II. EXPERIMENTAL SECTION

A. General

A description of the apparatus and experimental procedures is given elsewhere.[21] Briefly, ions are produced as described below and focused into a magnetic sector momentum analyzer for mass analysis. The mass-selected ions are decelerated to a desired kinetic energy and focused into an octopole ion guide that traps ions over the mass range studied. The octopole passes through a static gas cell into which reactant gases are introduced. After leaving the octopole, product and unreacted beam ions are focused into a quadrupole mass filter for product mass analysis. Ions are detected with a secondary electron scintillation ion detector and the signal is processed by pulse-counting techniques. Raw ion intensities are converted to absolute cross sections as described previously.[21]

Translational energies in the laboratory frame of reference are related to energies in the center-of-mass (CM) frame by $E_{CM}=E_{lab}m/(M+m)$, where M and m are the masses of the incident ion and neutral reactant, respectively. At low energies, the relative kinetic energy is corrected for the truncation of the ion beam. The absolute energy and the kinetic energy distribution of the ions in the interaction region are measured using the octopole as a retarding field analyzer.[21] The full width at half maximum of the energy distribution is 0.3–0.4 eV in the laboratory frame. Uncertainties in the absolute energy scale are ± 0.05 eV lab through most of the energy range included, but gradually increase at energies where the ion beam begins to be truncated, i.e., below about 0.8 eV lab in this work. The data obtained in this experiment are broadened by the ion energy distribution and thermal motion of the neutral gas. The second effect, referred to as Doppler broadening, has a width (in eV) in the CM frame of $0.4E^{1/2}-0.5E^{1/2}$ for these reactions.[22] This thermal energy is not included in the energy scales shown for the data but is explicitly included in all modeling of the reaction cross sections.[21]

Downloaded 11 Aug 2009 to 155.97.13.46. Redistribution subject to AIP license or copyright; see http://jcp.aip.org/jcp/copyright.jsp

B. Ion source

The data shown and analyzed in this paper involve the reactions of ions produced in a 1 m long flow tube[23] operating at a pressure of 0.6–0.8 Torr with a flow rate of 120–180 standard cm^3/s. Helium is used as the main flow gas, and water vapor diluted by He is added to the main flow. In this ion source, He^+ and He* are initially formed in a microwave discharge. Charge transfer and Penning processes ionize the water and sequential reactions form protonated water clusters that are thermalized by about 10^5 collisions with the room temperature carrier gas. Results for several systems[24–27] including $H(H_2O)_n^+$ $(n=1-5)$ (Ref. 14) indicate that these ions are efficiently thermalized under these conditions. Here, we verified that addition of Ar (up to 10% of the flow gas) did not change appreciably the cross sections associated with collision-induced dissociation of the proton-bound water clusters with Xe. Further, the thermochemistry derived below is consistent with thermalized clusters.

C. Theoretical analysis

For exothermic reaction channels, the cross sections are compared with those predicted by simple models: the Langevin–Gioumousis–Stevenson model,[28] $\sigma_{LGS} = \pi q(2\alpha/E)^{1/2}$, and the ion-locked dipole limit, $\sigma_{LD} = \sigma_{LGS} + \pi q(\mu_D/E)$,[29] where E is the collision energy, q is the charge on the electron, and α and μ_D are the polarizability (1.45 Å^3) and dipole moment (1.84 D) of water, respectively.[30] A more sophisticated model utilizes a parametrization of the kinetic energy dependence of ion-polar molecule collision rate constants determined by trajectory calculations. We use the formula $\sigma_{TR} = \sigma_{LGS} K_c$ where K_c is calculated using an expression given by Su[31] and depends on μ_D, α, and T_R, the rotational temperature, assumed to be 300 K here.

The energy dependence and thresholds for endothermic reactions are analyzed in the following way. Theory and experiment[32,33] show that cross sections can be parametrized in the threshold region using

$$\sigma(E) = \sigma_0 \Sigma g_i (E - E_0 + E_i + E_{rot})^N / E, \quad (1)$$

where the sum is over all vibrational states of the reactants denoted by i, g_i is the population of those states $(\Sigma g_i = 1)$, E_i is the excitation energy of each vibrational state of the reactant ion, E_{rot} is the average rotational energy of both reactants, σ_0 is an energy-independent scaling factor, E is the relative translational energy of the reactants, E_0 is the threshold for reaction of the ground rovibrational and electronic state of the reactants, and N is an adjustable parameter. As in previous work,[17,18] we assume that the complexes are in their ground electronic states. In the absence of evidence to the contrary, it is assumed that N and σ_0 are the same for all vibrational states. This form is expected to be appropriate for translationally driven reactions[34] and has been found to reproduce the cross sections for endothermic reactions in a number of previous studies of both atom-diatom and polyatomic reactions.[32,35] Although the $H(H_2O)_n^+$ clusters studied here are believed to be thermalized at room temperature, such weakly bonded cluster ions have low frequency vibrational modes whose populations are not negligible even at 300 K. Equation (1) takes these explicitly into account, as detailed elsewhere.[25]

TABLE I. Vibrational frequencies (cm^{-1}). Except where noted, values for $H_{2x+1}O_x^+$ species are from Ref. 17, and those for $D_{2x+1}O_x^+$ species are estimated as outlined in the text. Values in bold are taken from MP2(full)/6-311+G(2*d*,2*p*) calculations, see text.

Species	Frequencies (degeneracies)
H_2O[a]	3756, 3652, 1595; **3986**, **3866**, **1661**
D_2O[a]	2788, 2671, 1178
H_3O^+	3530, 3514(2), 1715(2), 910; **3719**, **3717**, **3611**, **1714(2)**, **907**
D_3O^+	2577, 2565(2), 1252(2), 664
$H_5O_2^+$	4045, 4044, 3934, 3922, 1884, 1834, 1698(2), 690, 639, 601(2), 510(2), 214 **3878**, **3877**, **3783**, **3775**, **1777**, **1735**, **1590**, **1515**, **804**, **622**, **545**, **543**, **466**, **294**, **175**
$D_5O_2^+$	2953, 2952, 2871, 2863, 1375, 1339, 1240(2), 504, 639, 601(2), 510(2), 214
$H_7O_3^+$	4086, 4083, 4034, 3962, 3961, 2755, 2629, 1871, 1828, 1801, 1779, 1405, 1261, 672, 561, 512, 478, 439, 412, 385, 374, 125, 107, 91
$D_7O_3^+$	2983, 2981, 2945, 2892, 2891, 2011, 1919, 1366, 1334, 1315, 1299, 1026, 1261, 672, 561, 512, 478, 439, 412, 385, 374, 125, 107, 91
$H_9O_4^+$	4096(2), 4094, 3968, 3967, 3966, 3192, 3147, 3137, 1915, 1886, 1797, 1793, 1792, 1333, 1128, 1065, 826, 515, 511, 446, 431, 410, 394, 375, 374, 282, 129, 110, 91, 75, 74, 66
$D_9O_4^+$	2990(2), 2989, 2897, 2896, 2895, 2330, 2297, 2290, 1398, 1377, 1311, 1309, 1308, 973, 1128, 1065, 826, 515, 511, 446, 431, 410, 394, 375, 374, 282, 129, 110, 91, 75, 74, 66
TS[b]	**3910**, **3814**, **3751**, **3590**, **3578**, **1710**, **1651**, **1650**, **1098**, **442**, **436**, **349**, **319**, **280**, **−469**

[a]Reference 37.
[b]Transition state for proton exchange in $H_5O_2^+$ shown in Fig. 6.

The Beyer–Swinehart algorithm[36] is used to evaluate the density of the ion vibrational states, and the relative populations g_i are calculated by the appropriate Maxwell–Boltzmann distribution at 300 K. Vibrational frequencies for H_2O and D_2O are taken from Shimanouchi.[37] Those for the proton-bound water clusters are taken from *ab initio* calculations reported in our previous study of the reactions of $H(H_2O)_n^+$ with ND_3.[17] We used these values because they provide a complete and self-consistent set of frequencies. Within the harmonic oscillator approximation,[38] the frequencies of intramolecular vibrations of D_2O in $D(D_2O)_n^+$ can be estimated by scaling the frequencies of H_2O in $H(H_2O)_n^+$ using the ratio of reduced masses, $(\mu_{O\text{-}D}/\mu_{O\text{-}H})^{1/2}$. For intermolecular vibrational modes where the reduced mass ratios are close to unity, the same frequencies are used. The frequencies used are summarized in Table I.

Before comparison with the experimental data, the calculated cross section of Eq. (1) is convoluted over the ion beam and neutral reactant kinetic energy distributions as described previously.[21] After convolution, the variable parameters σ_0, E_0, and N are optimized using a nonlinear least-squares analysis in order to best reproduce the data. We take the optimized value of E_0 to be the measured threshold for a particular data set. Uncertainties in the reported thresholds

Downloaded 11 Aug 2009 to 155.97.13.46. Redistribution subject to AIP license or copyright; see http://jcp.aip.org/jcp/copyright.jsp

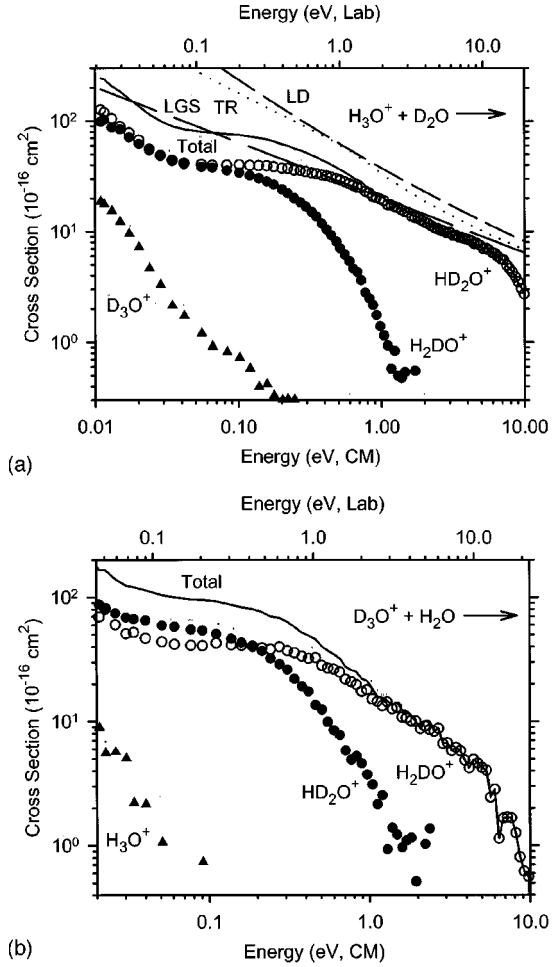

FIG. 1. Reaction cross sections for $H(H_2O)^+ + D_2O$ (part a) and $D(D_2O)^+ + H_2O$ (part b) as a function of collision energy in the center-of-mass frame (lower x axis) and laboratory frame (upper x axis). Lines show the total experimental cross section (full line), the Langevin–Gioumousis–Stevenson prediction (LGS, long dashed line), the locked-dipole prediction (LD, short dashed line), and the trajectory calculation (TR, dotted line). The neutral reagent pressure is 0.005 Torr in part a and 0.028 Torr in part b.

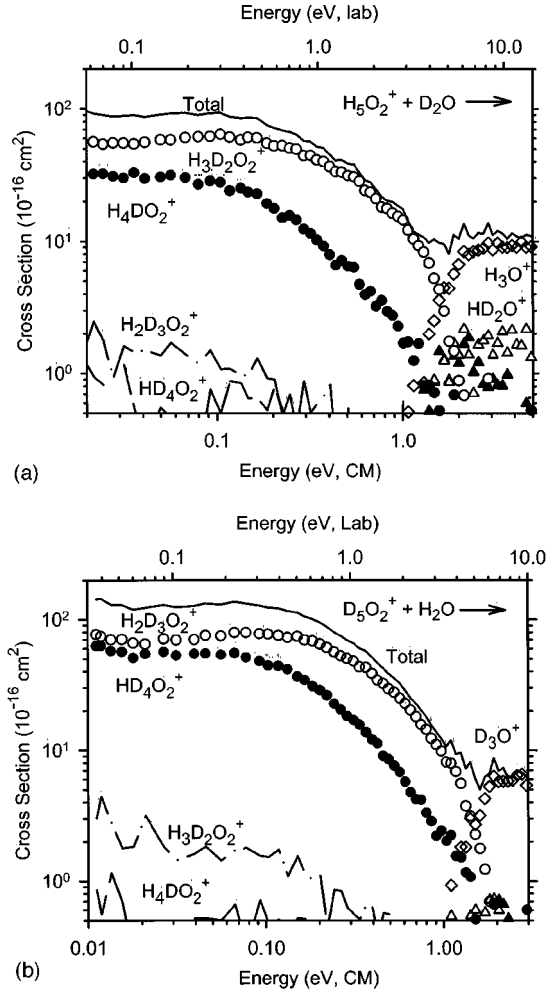

FIG. 2. Reaction cross sections for $H(H_2O)_2^+ + D_2O$ (part a) and $D(D_2O)_2^+ + H_2O$ (part b) as a function of collision energy in the center-of-mass frame (lower x axis) and laboratory frame (upper x axis). The full line shows the total product cross section. The neutral reagent pressure is 0.032 Torr in part a and 0.008 Torr in part b.

are derived from the spread of values for different data sets and the absolute uncertainty of the energy scale.

D. Results

Experimental results are summarized in Figs. 1–4 for $H(H_2O)_n^+$ ($n=1-4$) + D_2O (part a) and for $D(D_2O)_n^+$ ($n=1-4$) + H_2O (part b). The individual systems are discussed in the following sections. There are several experimental difficulties that must be addressed in this work. First, in order to ensure efficient collection of all products, the mass resolution in the quadrupole mass filter is usually set as low as possible. This can lead to overlap of intensities from adjacent peaks. In the results shown here, the mass resolution has been set sufficiently high that such overlap is negligible or the cross sections are corrected by subtracting the overlap. This latter procedure is used only when the correction is unambiguous, which is facilitated by the different energy dependences of various products. Second, the primary product ions can react to form additional products in secondary processes. This is addressed as discussed below. Third, the pressure of the neutral water reagent is difficult to control with high precision such that absolute cross sections reported here may have uncertainties of up to a factor of 2.

1. $H(H_2O)^+ + D_2O$

Figure 1(a) shows that reaction of $H(H_2O)^+$ with D_2O yields two products corresponding to processes (2a) and (2b).

$$H(H_2O)^+ + D_2O \rightarrow HD_2O^+ + H_2O \quad (2a)$$

$$\rightarrow H_2DO^+ + HDO. \quad (2b)$$

These two reactions are nearly thermoneutral, differing only in zero-point energies.[39] This is consistent with the observation that no energy threshold is observed for either process. The cross sections of reactions (2a) and (2b) decrease with increasing collision energy, such that the branching ratio remains fixed until about 0.1 eV. There, the cross section for reaction (2a) becomes more pronounced. Reaction (2a) is a simple proton transfer process but it also corresponds to exchange of a H_2O moiety for D_2O. In the larger systems

Downloaded 11 Aug 2009 to 155.97.13.46. Redistribution subject to AIP license or copyright; see http://jcp.aip.org/jcp/copyright.jsp

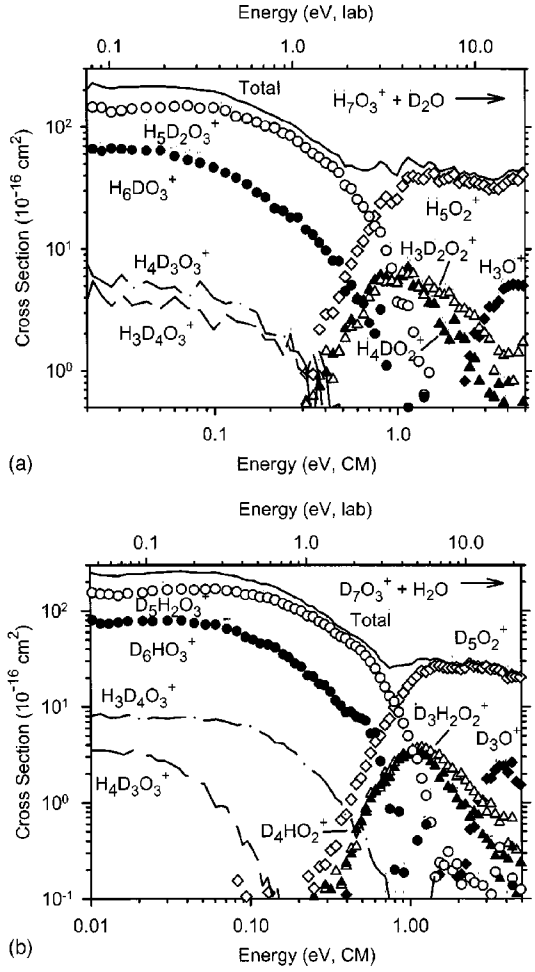

FIG. 3. Reaction cross sections for $H(H_2O)_3^+ + D_2O$ (part a) and $D(D_2O)_3^+ + H_2O$ (part b) as a function of collision energy in the center-of-mass frame (lower x axis) and laboratory frame (upper x axis). The full line shows the total product cross section. The neutral reagent pressure is 0.016 Torr in part a and 0.020 Torr in part b.

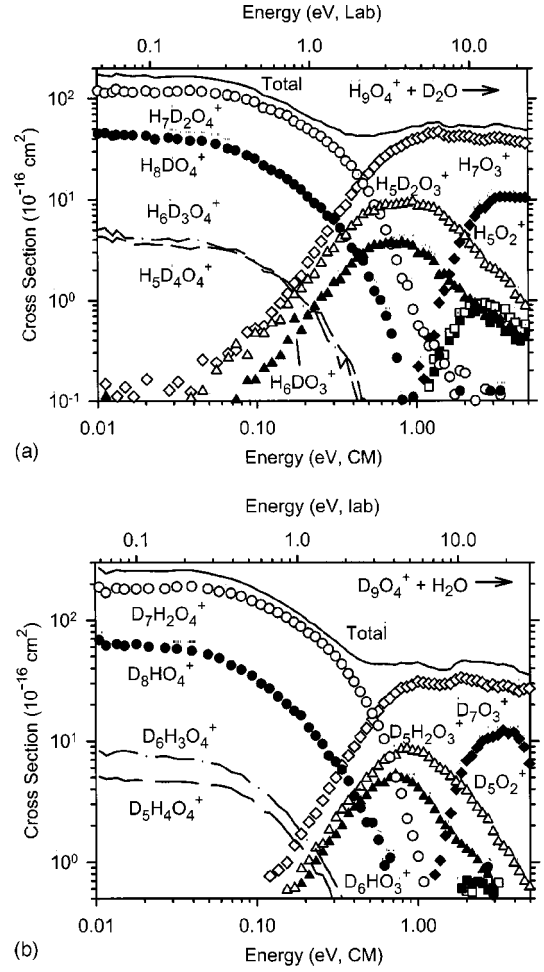

FIG. 4. Reaction cross sections for $H(H_2O)_4^+ + D_2O$ (part a) and $D(D_2O)_4^+ + H_2O$ (part b) as a function of collision energy in the center-of-mass frame (lower x axis) and laboratory frame (upper x axis). The full line shows the total product cross section. The neutral reagent pressure is 0.020 Torr in part a and 0.015 Torr in part b.

discussed below, this type of exchange process is the dominant reaction, which we refer to as "solvent exchange."

At low collision energies D_3O^+ was also observed. This is obviously a secondary collision product, as verified by determining that this cross section has a linear dependence upon the D_2O pressure. D_3O^+ can be formed by reactions of both H_2DO^+ and HD_2O^+ as shown in the following:

$$H_2DO^+ + D_2O \rightarrow D_3O^+ + H_2O \tag{2c}$$

$$\rightarrow HD_2O^+ + HDO, \tag{2d}$$

$$HD_2O^+ + D_2O \rightarrow D_3O^+ + HDO. \tag{2e}$$

Because the extent of these secondary processes is so small in the data shown in Fig. 1, the cross sections for the two primary products are quantitatively correct in the limit of single collisions, except at the very lowest energies.

In Fig. 1(a), the cross sections derived from the Langevin–Gioumousis–Stevenson (LGS) model, locked-dipole (LD) model, and trajectory (TR) calculation are indicated. The total cross section is smaller than the locked-dipole limit which is only an upper limit for ion-dipole collision cross sections. The total cross section generally falls between σ_{LGS} and σ_{TR}, which seems reasonable, especially when it is realized that the total cross section for reaction does not include the return to reactants, a process having nearly equivalent energetics to reactions (2). Similar observations apply to all systems studied here.

2. $D(D_2O)^+ + H_2O$

Cross sections for the reaction of D_3O^+ with H_2O are shown in Fig. 1(b). The primary products correspond to reactions (3a) and (3b).

$$D_3O^+ + H_2O \rightarrow H_2DO^+ + D_2O \tag{3a}$$

$$\rightarrow HD_2O^+ + HDO. \tag{3b}$$

At low collision energies H_3O^+ is observed. This is a secondary product formed in reaction (3c), as verified by its dependence on the pressure of H_2O.

$$D_3O^+ + 2H_2O \rightarrow H_3O^+ + D_2O + HDO. \tag{3c}$$

Reactions (3a) and (3b) have cross sections with comparable magnitudes at low energies, but as the collision energy in-

Downloaded 11 Aug 2009 to 155.97.13.46. Redistribution subject to AIP license or copyright; see http://jcp.aip.org/jcp/copyright.jsp

creases, the relative importance of the two channels switches such that the solvent exchange reaction product H_2DO^+ is dominant.

3. $H(H_2O)_n^+ + D_2O$ ($n=2-4$)

Figures 2–4 (part a) show cross sections for reaction of $H(H_2O)_n^+$ ($n=2-4$) with D_2O. In all systems, there are two primary products formed at low energies in the near thermoneutral reactions (4a) and (4b).

$$H(H_2O)_n^+ + D_2O \rightarrow H_{2n-1}D_2O_n^+ + H_2O \quad (4a)$$

$$\rightarrow H_{2n}DO_n^+ + HDO. \quad (4b)$$

In all cases, simple solvent exchange, reaction (4a), is favored at all energies. Each of these primary products can then undergo the following secondary reactions:

$$H_{2n-1}D_2O_n^+ + D_2O \rightarrow H_{2n-3}D_4O_n^+ + H_2O \quad (4c)$$

$$\rightarrow H_{2n-2}D_3O_n^+ + HDO, \quad (4d)$$

$$H_{2n}DO_n^+ + D_2O \rightarrow H_{2n-2}D_3O_n^+ + H_2O \quad (4e)$$

$$\rightarrow H_{2n-1}D_2O_n^+ + HDO. \quad (4f)$$

The $H_{2n-1}D_2O_n^+$ product ion of reaction (4f) is identical to one of the primary products and is therefore obscured. The ionic products formed in reactions (4c)–(4e) are observed in all three systems. It was verified that these $H_{2n-2}D_3O_n^+$ and $H_{2n-3}D_4O_n^+$ products are formed in secondary reactions by examining the dependence of the cross sections on the D_2O pressure. Because the extent of these secondary processes is so small in the data shown in Figs. 2–4, the cross sections for the primary products are quantitatively correct in the limit of single collisions, except perhaps at the very lowest energies.

As the collision energy is increased, the cross sections of the low energy products $H_{2n-1}D_2O_n^+$ and $H_{2n}DO_n^+$ decrease. In all cases, the decrease is more pronounced for $H_{2n}DO_n^+$, such that the solvent exchange reaction (4a) becomes more favorable as energy increases. Above about 1 eV, the endothermic reactions (4g)–(4i) are observed and eventually become dominant.

$$H(H_2O)_n^+ + D_2O \rightarrow H_{2n-1}O_{n-1}^+ + H_2O + D_2O \quad (4g)$$

$$\rightarrow H_{2n-2}DO_{n-1}^+ + H_2O + HDO \quad (4h)$$

$$\rightarrow H_{2n-3}D_2O_{n-1}^+ + 2H_2O. \quad (4i)$$

In all three systems, the simple collision-induced dissociation (CID) process (4g) has the largest cross section among these three reactions; the solvent exchange process (4i) is next in abundance; and the H-D scrambling process (4h) is least efficient. The magnitude of the cross section for reaction (4g) stays approximately constant at the highest energies, whereas those for reactions (4h) and (4i) decline. In the $n=3$ and 4 systems, we also observe additional products where one more H_2O molecule is removed from the products of reactions (4g)–(4i). Again the intensity of the product ion corresponding to simple CID, $H_{2n-3}O_{n-2}^+ + 2H_2O + D_2O$, is the largest.

4. $D(D_2O)_n^+ + H_2O$ ($n=2-4$)

Results for the reactions of $D(D_2O)_n^+$ ($n=2-4$) with H_2O are shown in Figs. 2–4 (part b). Comparison of these results with the analogous mirror reactions, $H(H_2O)_n^+ + D_2O$ ($n=2-4$), shows that the qualitative features are the same in all cases. The reactions involved are directly analogous to reactions (4a)–(4i).

E. Branching ratios

As we have seen in the previous sections, the primary product distribution at low energies is perturbed by secondary reactions of these products. In order to estimate the intrinsic branching ratios of these primary product channels, it is important to correct the data for the effect of these secondary reactions. In all systems, cross sections were determined at several pressures of the neutral reactant, and then these cross sections are extrapolated to values in the zero pressure limit. The branching ratios were determined using these extrapolated cross sections. At zero pressure, most secondary processes have cross sections within experimental error of being zero, which confirms that the extrapolation procedure is reasonable. Branching ratios at low kinetic energies ($0.04\,\text{eV} \approx 3k_BT/2$ at 298 K) determined after this extrapolation procedure are summarized in Table II.

III. DISCUSSION

A. Thermochemistry

Table III summarizes the threshold values and fitting parameters determined by analysis of the experimental cross sections with Eq. (1). Because all sources of energy are explicitly accounted for in these analyses, the E_0 thresholds determined in this work correspond to thermodynamic values at 0 K.[40] For comparison, Table III also lists values calculated from literature thermochemistry given in Tables IV and V. The solvation energies of the proton bound water clusters are usually given at 298 K, Table V. In order to obtain 0 K thermochemistry, we require the differences in heats of formation of the proton bound water clusters at 0 and 298 K, $\Delta_f H(0) - \Delta_f H(298)$. These were calculated from the heat capacities to be 9.6 kJ mol^{-1} for $H_5O_2^+$, 15.5 kJ mol^{-1} for $H_7O_3^+$, and 20.1 kJ mol^{-1} for $H_9O_4^+$ in the thermal electron convention.[17]

It can be seen in Table III that the thresholds determined here for the simple CID reactions of the $H(H_2O)_n^+$ clusters agree nicely with the literature values within experimental error. The good agreement indicates that molecularly bound neutral products, e.g., water dimer, are not formed to any appreciable extent because processes leading to these species would reduce the energy thresholds.[41] We can also ascertain thresholds for the simple CID reactions of the $D(D_2O)_n^+ + H_2O$ systems because these differ from those for the $H(H_2O)_n^+ + D_2O$ system by the differences in zero-point vibrational energies of the reactants and products. Using the vibrational frequencies listed in Table I, we obtain the literature values listed in Table III. Again the agreement with the measured thresholds is reasonable within the experimental uncertainties. Table III also shows that thresholds for formation of all isotopomers are very similar. For example, the

Downloaded 11 Aug 2009 to 155.97.13.46. Redistribution subject to AIP license or copyright; see http://jcp.aip.org/jcp/copyright.jsp

TABLE II. Branching ratios of the primary products at thermal energy.

Reactants	Products	This work[a]	SAH[b]	GBS[c]	AS[d]	Statistical[e]	Model[f]
$H_3O^+ + D_2O$	HD_2O^+/H_2DO^+	0.9±0.3	0.43	0.49	1.4	0.5	0.50
$H_5O_2^+ + D_2O$	$H_3D_2O_2^+/H_4DO_2^+$	1.5±0.3	1.00	0.85		1.0	1.33
$H_7O_3^+ + D_2O$	$H_5D_2O_3^+/H_6DO_3^+$	2.3±0.3		1.38		1.5	3.0,2.4[g]
$H_9O_4^+ + D_2O$	$H_7D_2O_4^+/H_8DO_4^+$	2.9±0.3				2.0	3.83
$D_3O^+ + H_2O$	DH_2O^+/D_2HO^+	1.0±0.2	0.54	0.61	0.92	0.5	0.50
$D_5O_2^+ + H_2O$	$D_3H_2O_2^+/D_4HO_2^+$	1.5±0.4	1.22	1.18		1.0	1.33
$D_7O_3^+ + H_2O$	$D_5H_2O_3^+/D_6HO_3^+$	2.2±0.3		1.65		1.5	3.0,2.4[g]
$D_9O_4^+ + H_2O$	$D_7H_2O_4^+/D_8HO_4^+$	3.3±0.5				2.0	3.83

[a]Values determined at 0.04 eV of collision energy from cross sections extrapolated to zero pressure reactant conditions. See text.
[b]Smith, Adams, and Henchman, Ref. 4.
[c]Graul, Brickhouse, and Squires, Ref. 42.
[d]Anicich and Sen, Ref. 7.
[e]The number of ways of producing an ion $H_aD_bO_n^+$ via the statistical decomposition of an intermediate $H_xD_yO_n^+$ is given by $[x!/(x-a)!a!]\cdot[y!/(y-b)!b!]$.
[f]The limiting values of X_2/X_3 when $\kappa = k_j/k_d = \infty$ in the kinetic scheme described in the text.
[g]See text.

thresholds of $H_7O_3^+$, $H_6DO_3^+$, and $H_5D_2O_3^+$ from $H_9O_4^+ + D_2O$ are the same within experimental uncertainties.

Another productive way of comparing the thresholds measured here to the literature is to convert them to solvation energies at 298 K. The converted values are summarized in Table V. Among literature values, the data set of Dalleska *et al.*[14] was determined by the collision-induced dissociation (CID) of $H(H_2O)_n^+$ clusters with Xe in our guided ion beam (GIB) mass spectrometer[12] and the other data sets were determined by thermal equilibrium measurements using high pressure mass spectrometry (HPMS).[10–13] The solvation energies determined here are in good agreement with either set of literature values.

B. Reaction mechanism and isotope scrambling

As mentioned in the Introduction, the hydrogen-bonded species, $H(H_2O)_n(D_2O)^+$ or $D(D_2O)_n(H_2O)^+$, are stable complexes. The reactions studied here can be understood by invoking these species as intermediates. The definition of an

TABLE III. Optimized parameters used in Eq. (1). Uncertainties in parentheses.

Reactant	Product	N	σ_0	E_0 (eV)	Lit E_0[a] (eV)
$H(H_2O)_2^+$	H_3O^+	0.9 (0.2)	35.4 (4.8)	1.35 (0.07)	1.36 (0.13)
	H_2DO^+	0.6 (0.3)	8.1 (1.3)	1.27 (0.10)	
	HD_2O^+	0.8 (0.2)	9.4 (0.4)	1.20 (0.16)	
$H(H_2O)_3^+$	$H_5O_2^+$	0.8 (0.1)	135 (14)	0.78 (0.04)	0.84 (0.10)
	$H_4DO_2^+$	0.5 (0.3)	23 (10)	0.73 (0.02)	
	$H_3D_2O_2^+$	0.6 (0.2)	32 (11)	0.71 (0.04)	
	H_3O^+	0.9 (0.1)	26 (5)	2.46 (0.32)	2.21 (0.17)
$H(H_2O)_4^+$	$H_7O_3^+$	0.6 (0.1)	157 (7)	0.66 (0.02)	0.70 (0.08)
	$H_6DO_3^+$	0.4 (0.2)	24 (4)	0.62 (0.03)	
	$H_5D_2O_3^+$	0.4 (0.1)	48 (20)	0.61 (0.02)	
	$H_5O_2^+$	1.2 (0.3)	48 (6)	1.51 (0.17)	1.55 (0.13)
	$H_4DO_2^+$	0.7 (0.1)	6.5 (0.4)	1.36 (0.14)	
	$H_3D_2O_2^+$	0.8 (0.1)	7.9 (0.5)	1.37 (0.14)	
$D(D_2O)_2^+$	D_3O^+	0.7 (0.2)	23 (8)	1.29 (0.11)	1.40 (0.13)
	D_2HO^+	0.7 (0.1)	2.8 (0.2)	1.28 (0.06)	
	DH_2O^+	0.7 (0.1)	1.6 (0.3)	1.28 (0.04)	
$D(D_2O)_3^+$	$D_5O_2^+$	0.7 (0.1)	80 (8)	0.82 (0.02)	0.83 (0.10)
	$D_4HO_2^+$	0.5 (0.2)	19 (3)	0.75 (0.05)	
	$D_3H_2O_2^+$	0.6 (0.2)	19 (4)	0.72 (0.08)	
	D_3O^+	0.6 (0.2)	10 (2)	2.37 (0.18)	2.24 (0.17)
$D(D_2O)_4^+$	$D_7O_3^+$	0.7 (0.1)	199 (25)	0.67 (0.01)	0.72 (0.08)
	$D_6HO_3^+$	0.3 (0.1)	28 (9)	0.66 (0.02)	
	$D_5H_2O_2^+$	0.3 (0.2)	52 (22)	0.67 (0.03)	
	$D_5O_2^+$	1.1 (0.2)	35 (6)	1.45 (0.16)	1.56 (0.13)
	$D_4HO_2^+$	0.6 (0.1)	1.5 (0.3)	1.46 (0.21)	
	$D_3H_2O_2^+$	0.6 (0.1)	1.2 (0.2)	1.39 (0.09)	

[a]Derived from median values in Table V.

Downloaded 11 Aug 2009 to 155.97.13.46. Redistribution subject to AIP license or copyright; see http://jcp.aip.org/jcp/copyright.jsp

TABLE IV. Heats of formation of relevant species. Unless otherwise noted, all values are taken from the JANAF Tables [M. W. Chase, C. A. Davies, J. R. Downey, D. J. Frurip, R. A. McDonald, and A. N. Syverud, J. Phys. Chem. Ref. Data, **14**, Suppl. 1].

Species	$\Delta_f H_{298}$ (kJ mol^{-1})	$\Delta_f H_0$ (kJ mol^{-1})
H	217.999±0.004	216.035±0.004
D	221.720±0.004	219.807±0.004
H^+	1536.25±0.04	1528.08±0.04
D^+	1540.32±0.04	1532.21±0.04
H_2O	−241.83±0.04	−238.92±0.04
D_2O	−249.20±0.07	−246.25±0.07
HDO	−245.37±0.06	−242.44±0.06
H_3O^+	597.8±8[a]	597.0±8[b]

[a]On the basis of $PA_{298}(H_2O)=697\pm8$ kJ mol^{-1} from S. G. Lias, J. F. Liebman, and R. D. Levin, J. Phys. Chem. Ref. Data **13**, 695 (1984).
[b]The 0 K value is obtained using information in the JANAF Tables.

intermediate complex can be considered within two types of experimental time scales. In the first, usually associated with cross-beam studies, a complex is usually identified as a species lasting for more than a rotational period. Work of Ryan *et al.*[1] shows that such a long-lived complex occurs for the $H_3O^+ + D_2O$ reaction at 0.7 eV but not above 2 eV. Although this study was not sensitive to the isotope scrambling channel, formation of $H_2DO^+ + HDO$, at the higher collision energies, the present work clearly shows that isotope scrambling persists up to fairly high collision energies. Such scrambling requires an intermediate that lives sufficiently long so that hydrogen migration occurs, i.e., for vibrational periods. It is in this context that we will refer to an intermediate complex.

At low energies, the extent of isotopic scrambling is represented by the branching ratios between reactions (2a) and (2b), (4a) and (4b), or the deuterated analogs. These are summarized in Table II along with results from three other experimental studies: the SIFT measurements of Smith, Adams, and Henchman (SAH),[4] the CID study of partially deuterated water cluster ions by Graul, Brickhouse, and Squires (GBS),[42] and the tandem ICR study by Anicich and Sen.[7] Table II also lists the statistical branching ratios expected for complete equilibration in a long-lived intermediate complex. In all systems, there are two primary products formed at low energies in reactions (4a) and (4b). The number of ways of producing an ion $H_aD_bO_n^+$ via the statistical decomposition of a $H_{2n+1}D_2O_{n+1}^+$ intermediate (or $D_aH_bO_n^+$ from $D_{2n+1}H_2O_{n+1}^+$) is given by $[(2n+1)!/(2n+1-a)!a!] \times [2!/(2-b)!b!]$. Thus, the relative, statistical probability of reaction (4a) versus (4b) is $n/2$.

Branching ratios for the systems measured here do not agree with either the statistical predictions or the results of SAH or GBS, Table II. For the present results and those of Anicich and Sen,[7] the ratios are larger than statistical, i.e., solvent exchange is favored over HDO loss. These differences can be rationalized as follows. In the CID study of GBS, thermally and isotopically equilibrated cluster ions are formed, mass selected, and then collisionally activated. In comparing these results with ours, it should be remembered that the deuterated clusters are formed under equilibrated conditions unlike the introduction of another isotope in a single collision. Further, the collisional excitation is at sufficiently high energies (>3 eV in the center of mass frame) that rearrangements of the clusters are unlikely and loss of peripheral water molecules is favored. In the experiment of SAH, the water clusters are allowed to reach an equilibrium distribution by allowing multiple collisions between the protonated water clusters and H_2O and D_2O. This permits more opportunities for the more extensive rearrangements required to yield HDO loss. In the tandem ICR work of Anicich and Sen,[7] many fewer collisions occurred, leading to results that roughly correspond with the single collision conditions employed in the present studies. Under these conditions, a more insightful analysis is possible for the details of the mechanism for proton exchange in these systems. In the following section, we describe a kinetic model which enable us to obtain such details of the mechanism.

TABLE V. Energies of solvation at 298 K (kJ mol^{-1}). Uncertainties are in parentheses.

Solvation energy	$n=2$	$n=3$	$n=4$	Source[a]
$D[H(H_2O)_{n-1}^+\text{-}H_2O]$	132 (6)	82 (4)	73 (4)	HPMS, CPK[b]
	133 (4)	79 (4)	74 (4)	HPMS, MS[c]
	138 (6)	88 (6)	67 (6)	HPMS, MF[d]
	146 (6)	85 (6)		HPMS, HTY[e]
	136 (6)	86 (5)	70 (5)	GIB, DHA[f]
	132 (7)	78 (4)	65 (2)	GIB, This work[g]
$D[D(D_2O)_{n-1}^+\text{-}D_2O]$	132 (11)	82 (2)	66 (1)	GIB, This work[g]

[a]HPMS=high pressure mass spectrometry. GIB=guided ion beam mass spectrometry.
[b]Cunningham, Payzant, and Kebarle, Ref. 10.
[c]Meot-Ner and Speller, Ref. 11.
[d]Meot-Ner and Field, Ref. 12.
[e]Hiraoka, Takimoto, and Yamabe, Ref. 13. Uncertainties assumed to be 6 kJ mol^{-1}.
[f]Dalleska, Honma, and Armentrout, Ref. 14.
[g]These values have been converted to 298 K from threshold values in Table III. Differences in the solvation energies at 298 and 0 K are calculated to be 7.5, 2.9, and 1.7 kJ mol^{-1} for $n=2-4$, respectively. See text for more details. The same corrections are assumed for $D(D_2O)_n^+$.

1. $H_3O^+ + D_2O$ and $D_3O^+ + H_2O$

As reviewed in the introduction, the simplest reaction systems studied here, $H_3O^+ + D_2O$ and $D_3O^+ + H_2O$, have been studied extensively. Our results are consistent with the observations of Ryan *et al.* in a crossed-beam study.[1] These authors observed both reactions (2a) and (2b) at 0.7 eV, but only reaction (2a) was seen between 2 and 5 eV. Although evidence of a persistent (lasting for rotational periods) complex was found only at the lowest energy, Ryan *et al.*[1] also showed that both reactions (2a) and (2b) proceeded by the same mechanism and that there was no abrupt change in mechanism with energy.

Henchman, Smith, and Adams proposed a simple model for isotope-exchange reactions,[6] in which they introduced the kinetic variable, $\kappa = k_j/k_d$, where k_j and k_d are the rate constants for the proton/deuteron rearrangement and the dissociation of intermediates, respectively. The variable κ, which is identified as the average number of proton/deuteron jumps occurring during the lifetime of the intermediate, was estimated to be larger than 20 for their thermal conditions. Fur-

Downloaded 11 Aug 2009 to 155.97.13.46. Redistribution subject to AIP license or copyright; see http://jcp.aip.org/jcp/copyright.jsp

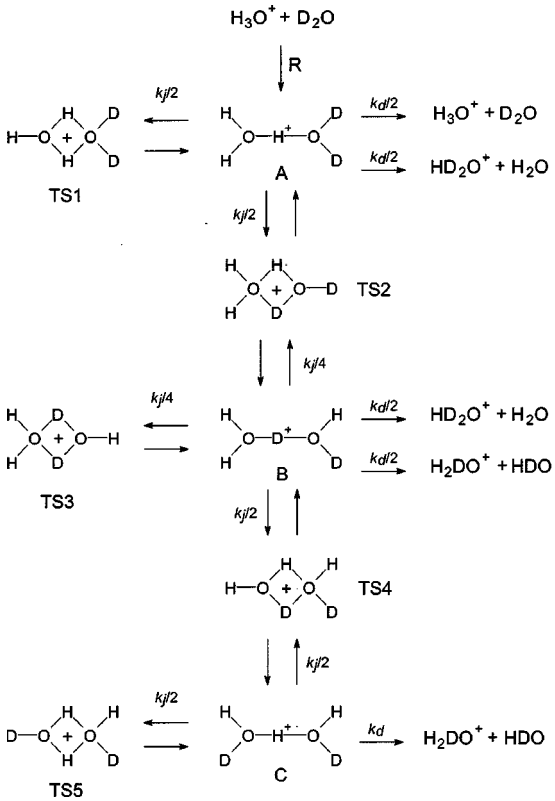

FIG. 5. Isomerization and dissociation scheme for the $H_3D_2O_2^+$ intermediate.

ther, they observed the same branching ratio at both 295 and 475 K.

The difficulty with the model proposed by Henchman, Smith, and Adams is that they postulated three intermediates, $H_3O^+ \cdot D_2O$ (I1), $H_2O \cdot HD_2O^+$ (I2), and $H_2DO^+ \cdot HDO$ (I3), which dissociate exclusively to $H_3O^+ + D_2O$, $HD_2O^+ + H_2O$, and $H_2DO^+ + HDO$, respectively. Although there are three distinct intermediates that are energetically similar (differing only in zero-point energies), quantum mechanical calculations[43] indicate that they are *A*, *B*, and *C* as shown in Fig. 5. Each of these three intermediates can dissociate in two ways, as shown in Fig. 5. As suggested by Evleth *et al.*,[43] we believe that interconversion of these intermediates occurs through the bridged structures shown as TS1–TS5 in Fig. 5. Calculations at a SCF/6-31G* level indicate that these bridged transition states lie 33.5 kJ/mol above the proton-bridged intermediates, *A*, *B*, and *C*.[43] These calculations also indicate that the binding energy of the $H_5O_2^+$ cluster (uncorrected for zero-point energies) is 137.7 kJ/mol, in good agreement with experimental values (Table V). Hence, these calculations indicate that the barrier to isomerization is well below that of dissociation.

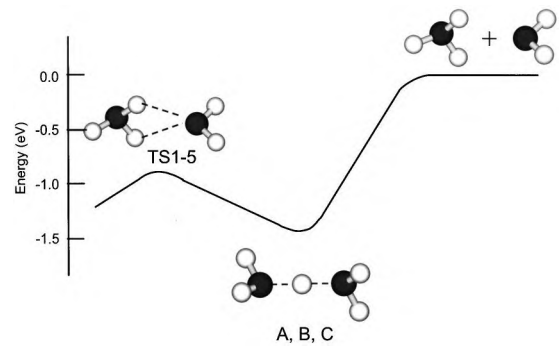

FIG. 6. Potential energy surface for proton exchange between two water molecules. Geometries of the products, intermediate, and transition state at the MP2(full)/6-311+G(2*d*,2*p*) level are shown and energies of the stationary points are calculated at the QCSID(T)/6-311+G(2*d*,2*p*)//MP2(full)/6-311+G(2*d*,2*p*) level.

To verify this suggestion and to obtain molecular constants necessary for the RRKM calculations described below, we also performed *ab initio* calculations of the $H_5O_2^+$ complex and the bridged transition state at the QCISD(T)/6-311+G(2*d*,2*p*)//MP2(full)/6-311+G(2*d*,2*p*) (Refs. 44–46) level of theory using GAUSSIAN 98.[47] Energetic and geometric results from these calculations are listed in Table VI, and Table I lists calculated vibrational frequencies. Figure 6 shows the potential energy surface and structures of the key intermediates and transition states. These calculations indicate that the transition state for hydrogen exchange lies 51.5 kJ/mol above the $H_5O_2^+$ ground state complex, which requires 136.9 kJ/mol to dissociate (where the energies include corrections for zero point energies). The latter is consistent with the experimental values of Table V.

In parallel with the treatment of Henchman, Smith, and Adams (HSA),[6] we assume that the isomerization steps

TABLE VI. *Ab initio* theoretical energies and structures.

Species	*R* (OH)[a] (Å)	∠(HOH)[a] (deg.)	∠(OHO)[a] (deg.)	QCISD(T)[b] (h)	ZPE (h)[c]	E_{rel} (eV)[d]
$H_5O_2^+$	0.964 (4)	108.9 (2)	173.9	−152.943 614	0.057 820	0.000
	1.195 (2)					
TS	0.962 (2)	104.8 (1)	106.0(2)	−152.926 733	0.060 549	0.534
	0.972 (1)	112.5 (2)				
	0.981 (2)	102.5 (1)				
H_3O^+	0.976 (3)			−76.582 093	0.035 045	1.419
H_2O	0.957 (2)			−76.308 264	0.021 674	

[a]Geometries calculated at the MP2(full)/6-311+G(2*d*,2*p*) level. Values in parentheses indicate how many of each structural element there are.
[b]Energies calculated at the QCSID(T)/6-311+G(2*d*,2*p*)//MP2(full)/6-311+G(2*d*,2*p*) level.
[c]Zero-point energies calculated at the MP2(full)/6-311+G(2*d*,2*p*) level.
[d]Relative values taken from the QCSID(T) results including ZPEs.

Downloaded 11 Aug 2009 to 155.97.13.46. Redistribution subject to AIP license or copyright; see http://jcp.aip.org/jcp/copyright.jsp

among A, B, and C have a uniform rate constant of k_j, whereas dissociation from A, B, or C has a uniform rate constant of k_d. The relative rates of the various steps are then shown in Fig. 5. Given this kinetic scheme and a rate for producing the initial complex R, it is straightforward to write the kinetic expressions for the three intermediates,

$$d[A]/dt = -(k_d + k_j/2)[A] + (k_j/4)[B] + R,$$

$$d[B]/dt = (k_j/2)[A] - (k_d + 3k_j/4)[B] + (k_j/2)[C],$$

$$d[C]/dt = (k_j/2)[B] - (k_d + k_j/2)[C].$$

If the steady state assumption is made for each of these intermediates and we use $\kappa = k_j/k_d$, then the solution to this set of equations is $[A] = (\kappa^2 + 10\kappa + 8)(R/k_d)/Z$, $[B] = 2\kappa(\kappa+2)(R/k_d)/Z$, $[C] = 2\kappa^2(R/k_d)/Z$, and $Z = (\kappa+2) \times (5\kappa+4)$ is the determinant of the matrix associated with the three equations above. To obtain rates for the products in the $H_3O^+ + D_2O$ system, the kinetic scheme of Fig. 5 predicts $d[H_3O^+]/dt = k_d[A]/2$, $d[HD_2O^+]/dt = k_d([A] + [B])/2$, $d[H_2DO^+]/dt = k_d([B] + 2[C])/2$. Integration of these expressions yields $[H_3O^+] = (\kappa^2 + 10\kappa + 8)(Rt/2Z)$, $[HD_2O^+] = (\kappa+4)(3\kappa+2)(Rt/2Z)$, and $[H_2DO^+] = 2\kappa(3\kappa+2)(Rt/2Z)$. HSA further reduce their comparable expressions to provide a reaction efficiency η, which excludes reformation of reactants, and then renormalize by dividing by η to obtain relative product distributions. This gives expressions for the branching fractions: $X_2 = [HD_2O^+]/\eta Rt$ and $X_3 = [H_2DO^+]/\eta Rt$, which are equivalent to $X_2 = [HD_2O^+]/([HD_2O^+] + [H_2DO^+])$ and $X_3 = [H_2DO^+]/([HD_2O^+] + [H_2DO^+])$, which are easily derived from experimental results. In terms of κ, HSA obtained the expressions: $X_2 = (\kappa+3)/(3\kappa+3)$, $X_3 = 2\kappa/(3\kappa+3)$, and $\eta = (9\kappa^2 + 9\kappa)/(10\kappa^2 + 21\kappa + 9)$, whereas the present kinetic scheme leads to $X_2 = (\kappa+4)/(3\kappa+4)$, $X_3 = 2\kappa/(3\kappa+4)$, and $\eta = (3\kappa+2)(3\kappa+4)/2Z = (9\kappa^2 + 18\kappa + 8)/(10\kappa^2 + 28\kappa + 16)$. These three expressions give the same limiting values as those of HSA when $\kappa \to \infty$, namely, $X_2 = 1/3$, $X_3 = 2/3$, and $\eta = 9/10$. The two expressions for X_2 and X_3 also give the same limiting values when $\kappa \to 0$, namely, $X_2 = 1$ and $X_3 = 0$, but the asymptotic values of η differ: 0 for the expression of HSA and 1/2 here. This latter difference is telling. As $\kappa \to 0$, k_j becomes small compared to k_d, i.e., the intermediates dissociate rapidly compared to the time needed for isomerization. In this limit, reactants form only the first intermediate (I1 or A in the two reaction schemes), and thus only the dissociation products of this intermediate will be observed. I1 dissociates exclusively back to reactants, hence the reaction efficiency falls to zero. Intermediate A dissociates to both the reactants and to the simple protron transfer product HD_2O^+. Experimentally, we and Ryan *et al.*[1] observe that the HD_2O^+ product is formed at elevated energies, i.e., the reaction efficiency is nonzero. This agrees with the present model and contrasts sharply with the predictions of the kinetic scheme of HSA, which can also be rejected on the basis of quantum mechanical calculations regarding the potential energy surfaces of these reactions.

It remains to explore the relationship between κ and kinetic energy. Empirically, we find there is less isomerization

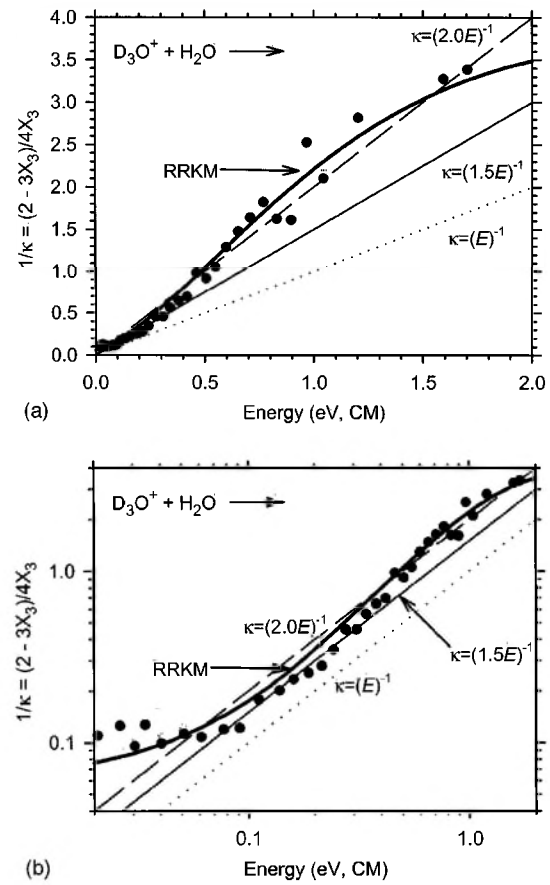

FIG. 7. $\kappa^{-1}(=k_d/k_j)$ calculated from the observed branching fractions are plotted as a function of collision energy in the center-of-mass frame for $D(D_2O)^+ + H_2O$. Also shown are three cases where κ^{-1} is proportional to E (dotted line), $1.5E$ (solid line), and $2E$ (broken line), respectively. The RRKM rate constant prediction is also shown as bold solid line.

as the kinetic energy of the reactants increases, indicating that k_j increases less rapidly than k_d with energy. This is sensible given that the activation energy for isomerization is about 51 kJ/mol, whereas that for decomposition is about 137 kJ/mol. Further, the intermediates have at least 137 kJ/mol of internal energy even at a collision energy of zero. Thus, κ should decrease as energy increases. This agrees qualitatively with the findings of Henchman, Smith, and Adams that κ varies as $T^{-1.5}$ for isotopic exchange observed in the $CH_5^+ + CD_4$ system.[6]

To obtain a more quantitative characterization of the kinetic energy dependence of κ, we rearrange the expressions for X_2 and X_3 to solve for $1/\kappa$. This yields $1/\kappa = (3X_2 - 1)/(4 - 4X_2)$ or equivalently, because $X_2 + X_3 = 1$, $1/\kappa = (2 - 3X_3)/4X_3$. The advantage of these formulas is that the experimental branching fractions as a function of kinetic energy can now be plotted to directly determine the kinetic energy dependence of κ. A plot of $1/\kappa$ calculated in this way from the data versus energy is shown in Fig. 7(a). Such plots are roughly linear from about 0.1 to 1.0 eV with intercepts close to zero. Linear regression analysis of the data yields average slopes (which depend on the energy range chosen) of 1.7 ± 0.3 for the $H_3O^+ + D_2O$ systems and 1.6 ± 0.6 for the $D_3O^+ + H_2O$ systems (and an overall average of 1.6 ± 0.4). Thus, the energy dependence of κ is approximately

Downloaded 11 Aug 2009 to 155.97.13.46. Redistribution subject to AIP license or copyright; see http://jcp.aip.org/jcp/copyright.jsp

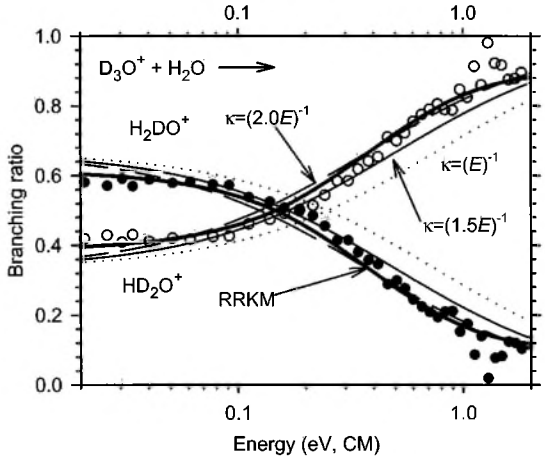

FIG. 8. Branching fractions of H_2DO^+ and HD_2O^+ formed by $D(D_2O)^+ + H_2O$ as a function of collision energy in the center-of-mass frame (lower x axis). Branching fractions of these products estimated from the model described in Fig. 5 are also shown as a function of $\kappa^{-1}(=k_d/k_j)$ (upper x axis). Dotted, solid, and broken lines correspond to the cases in which κ^{-1} is E, $1.5E$, and $2E$, respectively. The two bold solid lines are branching fractions predicted by the RRKM rate constants.

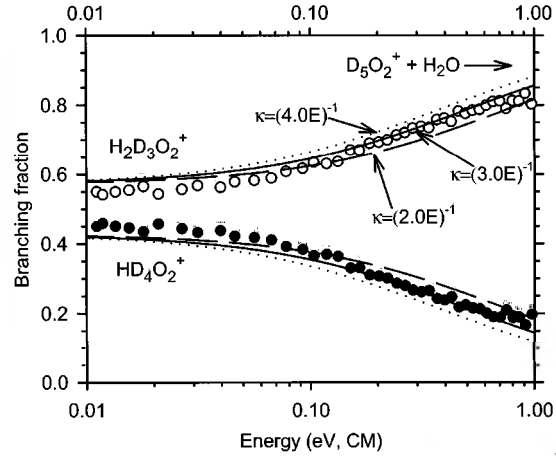

FIG. 9. Branching fractions of $H_2D_3O_2^+$ and $HD_4O_2^+$ formed by $D(D_2O)_2^+ + H_2O$ as a function of collision energy in the center-of-mass frame (lower x axis). Broken, solid, and dotted lines correspond to the cases in which κ^{-1} is $2E$, $3E$, and $4E$, respectively.

$(1.6E)^{-1}$, although Fig. 7(b) shows clearly that the data is really not linear. An alternative way of comparing the model to the data (which is more useful when the data cannot be directly transposed to $1/\kappa$, as for the larger clusters of $n \geqslant 3$) is shown in Fig. 8. Here, the energy dependence of the experimental branching fraction is compared to predictions assuming that κ is $(E)^{-1}$, $(1.5E)^{-1}$, and $(2E)^{-1}$. It can be seen that the line for $\kappa=(1.5E)^{-1}$ agrees with the data well over an energy range of about 0.05 to 0.5 eV, whereas $\kappa=(2E)^{-1}$ agrees better at higher energies. This is consistent with the comparison of the data to the same three models in Fig. 7.

Additional insight into the model can be obtained using RRKM statistical theory to calculate the rates of isomerization k_j and dissociation k_d. Using the theoretically calculated energies and frequencies (Tables I and VI), the energy dependence of these two rates can be determined straightforwardly and hence $1/\kappa=k_d/k_j$ can be calculated from first principles. We take the zero of energy to be the energy of the reactant asymptote plus any thermal energy of the reactants (to mimic the experimental conditions at zero kinetic energy), $6kT=0.15$ eV, and assume that the reaction path degeneracies are both unity. The energy variation of the RRKM predicted value of $1/\kappa$ is also shown in Figs. 7 and 8. It can be seen to be in excellent agreement with the data over an extended energy range. The RRKM prediction is nonlinear, which indicates that the number of states for the dissociation and isomerization pathways have a more complex dependence on energy than simply linear. As a consequence, the near-linear dependence of $1/\kappa$ versus E is largely serendipitous.

The calculated RRKM branching ratio at thermal energies (0.04 eV) is found to be 0.70, although the calculated asymptotic limit at 0 K remains 0.50 as predicted by the statistical and kinetic models, Table II. The predicted RRKM result is within experimental error of the branching ratios observed here, Table II. This agreement indicates that on the time scale of these experiments, the dissociation is sufficiently fast compared to the isomerization rate at low collision energies that complete isotopic equilibration does not occur even though the system is behaving statistically.

2. $H_{2n+1}O_n^+ + D_2O$ and $D_{2n+1}O_n^+ + H_2O$ ($n \geqslant 2$)

Given the remarkable agreement between the predictions of the kinetic model shown in Fig. 5 and the energy dependence of the branching fractions, Figs. 7 and 8, it seems reasonable to extend this model to the larger proton-bound water clusters. This is straightforwardly done for the case of $H_5O_2^+ + D_2O$ and $D_5O_2^+ + H_2O$. Here, there are seven intermediates coupled by the same kinds of transition states postulated in Fig. 5. In this case, the solution of the kinetic equations yields $X_2=[H_3D_2O_2^+]/\eta Rt=(2\kappa+3)(4\kappa+3)/(14\kappa^2+24\kappa+9)$, $X_3=[H_4DO_2^+]/\eta Rt=6\kappa(\kappa+1)/(14\kappa^2+24\kappa+9)$, and $\eta=(14\kappa^2+24\kappa+9)/2(2\kappa+3)(4\kappa+3)$. Again we can invert the data by finding $1/\kappa=(14X_2-8)/[9-12X_2+3(2X_2^2-2X_2+1)^{1/2}]$. Here the $1/\kappa$ versus E data are best fit for both isotopic variants with a slope of 3 ± 1 and small intercepts. This solution $\kappa=(3E)^{-1}$ is compared to the data for the $D_5O_2^+ + H_2O$ reaction in Fig. 9, and again the agreement can be seen to be very good. This agreement is also seen in the branching ratios at thermal energy, Table II. Again, this shows that statistical behavior is being observed in the present system even though complete isotopic equilibration is not achieved.

Extension of the kinetic model to the larger systems is more complicated. We first examine the case of the $H_9O_4^+ + D_2O$ and $D_9O_4^+ + H_2O$ reactions as these are simpler than the $H_7O_3^+ + D_2O$ and $D_7O_3^+ + H_2O$ systems. The full kinetic scheme for $H_9O_4^+ + D_2O$ is shown in Fig. 10, where it can be seen that there are again seven intermediates. One reason for this is that the central H_3O^+ is a bottleneck that does not allow the deuterium label to pass. Hence the intermediates in this system are comparable to those in the $H_5O_2^+ + D_2O$ system, however, dissociation of these intermediates can occur from three positions in these species. If we assume

Downloaded 11 Aug 2009 to 155.97.13.46. Redistribution subject to AIP license or copyright; see http://jcp.aip.org/jcp/copyright.jsp

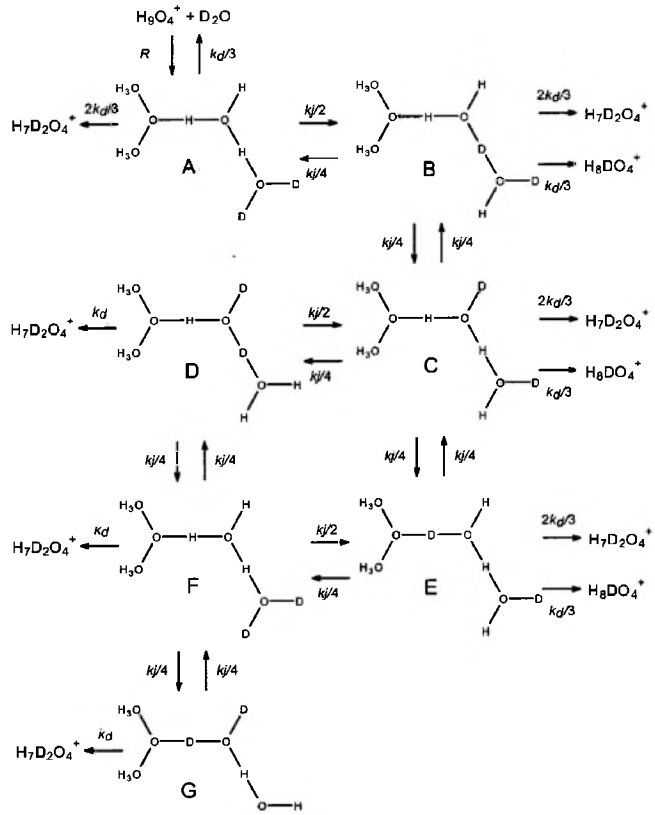

FIG. 10. Isomerization and dissociation scheme for the $H_9D_2O_5^+$ intermediate.

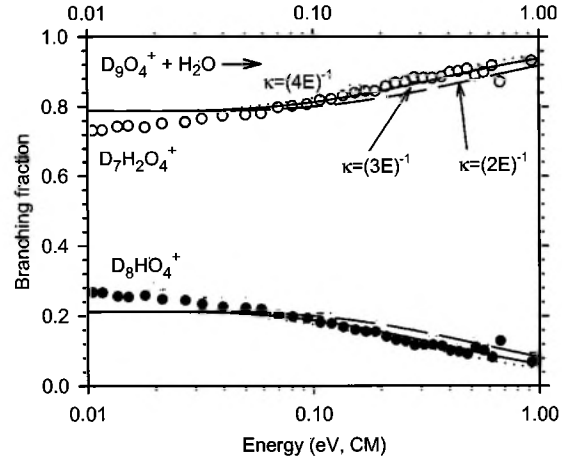

FIG. 11. Branching fractions of $H_7D_2O_4^+$ and $H_8DO_4^+$ formed by $H(H_2O)_4^+ + D_2O$ as a function of collision energy in the center-of-mass frame (lower x axis). Broken, solid, and dotted lines correspond to the cases in which κ^{-1} is $2E$, $3E$, and $4E$, respectively.

equal rates of dissociation from all three positions, this yields the results: $[H_7D_2O_4^+]/Rt = (115\kappa^6 + 1684\kappa^5 + 9008\kappa^4 + 22\,528\kappa^3 + 28\,416\kappa^2 + 17\,408\kappa + 4096)(2/3Z)$, $[H_8DO_4^+]/Rt = (30\kappa^6 + 488\kappa^5 + 2304\kappa^4 + 4416\kappa^3 + 3584\kappa^2 + 1024\kappa)(2/3Z)$, $\eta = (145\kappa^6 + 2172\kappa^5 + 11\,312\kappa^4 + 26\,944\kappa^3 + 32\,000\kappa^2 + 18\,432\kappa + 4096)(2/3Z)$, and $Z = (100\kappa^6 + 1600\kappa^5 + 8864\kappa^4 + 22\,464\kappa^3 + 28\,416\kappa^2 + 17\,408\kappa + 4096)$. Here it is impossible to transpose the measured branching fractions to κ, so instead branching fractions were calculated for several energy dependences of $1/\kappa$ and compared with the experimental values in Fig. 11. This shows that a $1/\kappa = (3 \pm 1)E$ dependence provides the best fit.

However, at lower energies, the deviation between the data and the prediction is pronounced. We ascribe this to the fact that dissociation from the three possible positions is not equivalent because the D_2O reactant adds to a second solvent shell around the central H_3O^+ unit. Energetically, loss of the outermost water from one position (out of three) should occur preferentially as this yields a $H_9O_4^+$ complex in its ground state structure. Among the seven possible intermediates, HDO loss is favored in three (B,C,E) and H_2O loss is favored in two (D and G). The other two intermediates (A and F) lead preferentially D_2O loss, i.e., back to the reactant. At lower energies, this preference should enhance the relative yield of the HDO loss process compared to that for H_2O loss. This preference is qualitatively in agreement with the observed branching fraction. This also explains why the branching ratio experimentally observed at thermal energies is smaller than the prediction of the kinetic model, Table II.

In the case of the $H_7O_3^+ + D_2O$ and $D_7O_3^+ + H_2O$ systems, there are two additional points of complexity. Now the incoming water reactant can add at two positions to the cluster ion, yielding two distinct intermediates. If the water reactant adds to the single central proton to form the ground state structure of $H_7D_2O_4^+$ (and $H_2D_7O_4^+$), the kinetics are quite simple as there are only two intermediates. This leads to the predictions that $[H_5D_2O_3^+]/\eta = (6\kappa+4)/(8\kappa+4)$, $[H_6DO_3^+]/\eta = (2\kappa)/(8\kappa+4)$, and $\eta = (8\kappa+4)/3(3\kappa+2)$. This predicts a branching ratio at thermal energy of 3.0 as listed in Table II. If the water reactant adds to one of the four outermost protons, the situation is considerably more complicated. Now there are 13 distinct but nearly equivalent intermediates. We have not completed the solution of this complex problem as the dichotomy between the likelihood of forming the two types of intermediates cannot be resolved in any direct manner. However, simple statistical consideration for these 13 intermediates predicts a branching ratio ($H_5D_2O_3^+/H_6HO_3^+$ or $D_5H_2O_3^+/D_6HO_3^+$) at thermal energies of 2.4, which is quite similar to the present experimental results, Table II. The 4:1 ratio of outer versus inner protons available to react may explain why the latter mechanism appears to be experimentally favored.

Recent *ab initio* calculations have proposed that the proton transfer in $H(H_2O)_3^+$ is an activated process involving reorganization of the cluster as a whole.[48,49] Therefore, for $n=2$, the H-D exchange processes may not be as simple as described in the kinetic model here. For $H_5O_2^+ + D_2O$ ($D_5O_2^+ + H_2O$), we have derived a model involving such reorganization, which involves transfer of water molecules that automatically includes H-D scrambling, and obtained quite similar results to the kinetic model discussed above. These calculations do not specifically address whether such reorganization may be important for larger systems ($n=3$ and 4). However, the H-D exchange process requires the mechanism described here, as reorganization alone cannot yield the H-D exchange results observed here, although reorganization could possibly augment the mechanism suggested here.

Downloaded 11 Aug 2009 to 155.97.13.46. Redistribution subject to AIP license or copyright; see http://jcp.aip.org/jcp/copyright.jsp

C. Energy dependence of the reaction cross sections

The total cross sections determined in this study for reaction of $H(H_2O)_n^+$ ($n=1-4$) with D_2O and the mirror reactions of $D(D_2O)_n^+$ ($n=1-4$) with H_2O are all smoothly decreasing functions of the collision energy, Figs. 1–4. Recently, Yamaguchi *et al.* measured reaction cross sections for $H(H_2O)_n^+ + D_2O$ ($n=2-11$) reactions over an energy range up to 2.0 eV by using guided ion beam techniques combined with a corona discharge ion source.[50] Cross sections for incorporation, reactions (4a) and (4b), versus dissociation, reactions (4g)–(4i), channels were determined, but results for individual isotopic channels are not reported. The absolute values and the collision energy dependence of the total cross sections agree with the results obtained by Yamaguchi *et al.* for $n=2$ to 4.[50]

At the lowest energies, the total cross sections fall close to σ_{LGS}, which is reasonable because this should be a lower limit to the collision cross section but the observed cross section does not include the back reaction to reform reactants. As the kinetic energy is further increased, the cross sections begin to decline more rapidly. In our study of the reactions of water clusters with acetonitrile, we attributed this to an inability to conserve angular momentum in the exit channel, a process that relies on a greater polarizability and dipole moment of acetonitrile than those of water. As the neutral products in the present reactions are always water molecules, such an explanation cannot be used here. We imagine that the decline must correspond to energies where the initial intermediate complex formation becomes increasingly less likely, as also indicated by large changes in the branching ratios for the $H_{2n-1}D_2O_n^+/H_{2n}DO_n^+$ and $D_{2n-1}H_2O_n^+/D_{2n}HO_n^+$ products in the same energy region. Similar considerations probably hold for the CH_3CN and ND_3 systems studied earlier.

At the highest kinetic energies, the total cross sections level off. It can be seen in Figs. 2–4 that the cross sections at these high energies are mainly a result of collision-induced dissociation reactions. Because the $H_3O^+ + D_2O$ and $D_3O^+ + H_2O$ reactions have no low-energy CID reaction channels, their cross sections do not level off at high energies. At these higher collision energies, the experimental cross sections should not be compared with σ_{LGS} or σ_{LD}, but rather with a hard sphere collision cross section σ_{HS}. For large ions such as the water clusters σ_{HS} can be appreciable, although it is difficult to estimate for nonspherical cluster ions. For instance, $H(H_2O)_4^+$ has a 3.6 Å radius in the molecular plane,[19] such that σ_{HS} is ~80 Å^2 if 1.4 Å is chosen as the radius of the neutral reactant. Because $H(H_2O)_4^+$ is a prolate symmetric top molecule, this value should be an upper limit to the experimental cross section. This is in qualitative agreement with the magnitudes of the cross sections in Fig. 4 at high energies, 50±10 Å^2. The $H(H_2O)^+$ ion is also a prolate symmetric top molecule and σ_{HS} of reaction (2) is estimated to be ~23 Å^2. The σ_{HS} cross sections for clusters of $n=2$ and 3 should be between these limits. As with the $n=4$ case, we observe somewhat smaller cross sections at the highest energies, approximately 9±2 Å^2 for $n=2$, Fig. 2, and 40±10 for $n=3$, Fig. 3.

IV. CONCLUSIONS

Reactions of protonated water clusters $H(H_2O)_n^+$ ($n=1-4$) with D_2O and their mirror reactions, $D(D_2O)_n^+$ ($n=1-4$), with H_2O are studied using guided-ion beam mass spectrometry. Absolute reaction cross sections are determined as a function of the collision energy from thermal energy to over 5 eV. At low collision energies, H-D exchange product ions are observed as well as solvent exchange reaction products. Relative ratios of the H-D exchange and solvent exchange products indicate that the reactions proceed by formation of an intermediate complex. With increasing collision energy, the H-D exchange products decrease and the solvent exchange products become dominant. At high collision energies, loss of one or two water molecules from the intermediate complex ions are the dominant processes, with simple collision-induced dissociation (CID) reactions providing most of the intensity. Some H-D exchange persists even at these energies, however. Threshold energies of endothermic channels were determined and binding energies of solvent molecules H_2O and D_2O are consistent with those determined by thermal equilibrium measurements[10–13] and previous collision-induced dissociation studies.[14]

A kinetic model based on realistic intermediate and transition states is introduced to explain the observed branching fractions for H-D and water exchange products. This model successfully accounts for the collision energy dependence of the branching fractions for all systems by using only one parameter, κ, the ratio of isomerization (k_j) and dissociation (k_d) rate constants. The feasibility of this kinetic model is verified by detailed *ab initio* calculations of the intermediate and transition states proposed for the $H_3O^+ + H_2O$ reaction coupled with RRKM calculations of k_j and k_d, which accurately predict the observed branching fractions. The parameterization in terms of κ allows a straightforward extension of this kinetic model to larger clusters, where it is also found to adequately predict the kinetic energy dependence of the reactions. Although some deviations do occur, these are easily rationalized.

ACKNOWLEDGMENTS

This research was supported by the National Science Foundation, Grant Nos. CHE-9877162 and 0135517.

[1] P. W. Ryan, C. R. Blakey, M. L. Vestal, and J. H. Futrell, J. Phys. Chem. **84**, 561 (1980).
[2] J. Rheinecker, T. Xie, and J. M. Bowman, J. Chem. Phys. **120**, 7018 (2004).
[3] N. G. Adams, D. Smith, and M. J. Henchman, Int. J. Mass Spectrom. Ion Phys. **42**, 11 (1982).
[4] D. Smith, N. G. Adams, and M. J. Henchman, J. Chem. Phys. **72**, 4951 (1980).
[5] M. Henchman and J. F. Paulson, J. Chem. Soc., Faraday Trans. 2 **85**, 1673 (1989).
[6] M. Henchman, D. Smith, and N. G. Adams, Int. J. Mass Spectrom. Ion Processes **109**, 105 (1991).
[7] V. G. Anicich and A. D. Sen, Int. J. Mass Spectrom. Ion Processes **172**, 1 (1998).
[8] J. E. Del Bene, M. J. Frisch, and J. A. Pople, J. Phys. Chem. **89**, 3669 (1985).
[9] R. Remington and H. F. Schaefer, as cited in L. I. Yeh, M. Okumura, J. D. Myers, J. M. Price, and Y. T. Lee, J. Chem. Phys. **91**, 7319 (1989).
[10] A. J. Cunningham, J. D. Payzant, and P. Kebarle, J. Am. Chem. Soc. **94**,

Downloaded 11 Aug 2009 to 155.97.13.46. Redistribution subject to AIP license or copyright; see http://jcp.aip.org/jcp/copyright.jsp

7627 (1972); Y. K. Lau, S. Ikuta, and P. Kebarle, *ibid.* **104**, 1462 (1982).
[11] M. Meot-Ner and C. V. Speller, J. Phys. Chem. **90**, 6616 (1986).
[12] M. Meot-Ner and F. H. Field, J. Am. Chem. Soc. **99**, 998 (1977).
[13] K. Hiraoka, H. Takimoto, and S. Yamabe, J. Phys. Chem. **90**, 5910 (1986).
[14] N. F. Dalleska, K. Honma, and P. B. Armentrout, J. Am. Chem. Soc. **115**, 12125 (1993).
[15] A. W. Castleman and R. G. Keesee, Science **241**, 36 (1988).
[16] P. M. Hierl, A. F. Ahren, M. J. Henchman, A. A. Viggiano, J. F. Paulson, and D. C. Clary, Faraday Discuss. Chem. Soc. **85**, 37 (1988).
[17] K. Honma, L. S. Sunderlin, and P. B. Armentrout, Int. J. Mass Spectrom. Ion Processes **117**, 237 (1992).
[18] K. Honma, L. S. Sunderlin, and P. B. Armentrout, J. Chem. Phys. **99**, 1623 (1993).
[19] M. Meot-Ner, J. Am. Chem. Soc. **106**, 1265 (1984); C. A. Deakyne, M. Meot-Ner, C. L. Campbell, M. G. Hughes, and S. P. Murphy, J. Chem. Phys. **84**, 4958 (1986).
[20] In the case of reactions with CH_3CN, the CH_3^+ ion was also observed at high collision energies.
[21] K. M. Ervin and P. B. Armentrout, J. Chem. Phys. **83**, 166 (1985).
[22] P. J. Chantry, J. Chem. Phys. **55**, 2746 (1971).
[23] R. H. Schultz and P. B. Armentrout, Int. J. Mass Spectrom. Ion Processes **107**, 29 (1991).
[24] E. R. Fisher and P. B. Armentrout, J. Chem. Phys. **94**, 1150 (1991).
[25] R. H. Schultz, K. C. Crellin, and P. B. Armentrout, J. Am. Chem. Soc. **113**, 8590 (1991).
[26] E. R. Fisher, B. L. Kickel, and P. B. Armentrout, J. Chem. Phys. **97**, 4859 (1992).
[27] M. T. Rodgers and P. B. Armentrout, J. Phys. Chem. A **101**, 1238 (1997).
[28] G. Gioumousis and D. P. Stevenson, J. Chem. Phys. **29**, 294 (1958).
[29] T. F. Moran and W. H. Hammill, J. Chem. Phys. **39**, 1413 (1963).
[30] E. W. Rothe and R. B. Bernstein, J. Chem. Phys. **31**, 1619 (1959).
[31] T. Su, J. Chem. Phys. **100**, 4703 (1994).
[32] See, for example, N. Aristov and P. B. Armentrout, J. Am. Chem. Soc. **108**, 1806 (1986).
[33] P. B. Armentrout, *Advances in Gas Phase Ion Chemistry*, edited by N. G. Adams and L. M. Babcock (JAI, Greenwich, 1992), Vol. 1, p. 83.
[34] W. J. Chesnavich and M. T. Bowers, J. Phys. Chem. **83**, 900 (1979).
[35] See, for example, L. S. Sunderlin and P. B. Armentrout, Int. J. Mass Spectrom. Ion Processes **94**, 149 (1989).
[36] T. Beyer and D. F. Swinehart, Comm. Assoc. Comput. Machinery **16**, 379 (1973); S. E. Stein and B. S. Rabinovitch, J. Chem. Phys. **58**, 2438 (1973); Chem. Phys. Lett. **49**, 183 (1977); R. G. Gilbert and S. C. Smith, *Theory of Unimolecular and Recombination Reactions* (Blackwell Science, Oxford, 1990).
[37] T. Shimanouchi, Consolidation Vol. I NSRDS-NBS 39, 1972.
[38] See for example, G. Herzberg, *Molecular Spectra and Molecular Structure, I. Spectra of Diatomic Molecules* (Van Nostrand, New York, 1950).
[39] M. Henchman, D. Smith, and N. G. Adams, Int. J. Mass Spectrom. Ion Phys. **42**, 25 (1982). Estimated $\Delta_r H^0$ for reactions (2a) and (2b) and the "mirror" reactions from the zero-point energies as endothermic by 0.8 and 0.4 kJ/mol, respectively.
[40] Internal energies of neutral reactants H_2O or D_2O were not accounted for but should be small.
[41] Water dimer formation would reduce the energy threshold by 0.17 eV. M. J. Frisch, J. A. Pople, and J. E. Del Bene, J. Phys. Chem. **89**, 3664 (1985).
[42] S. T. Graul, M. D. Brickhouse, and R. R. Squires, J. Am. Chem. Soc. **112**, 631 (1990).
[43] E. M. Evleth, Z. D. Hamou-Tahra, and E. Kassab, J. Phys. Chem. **95**, 1213 (1991).
[44] C. Møller and M. S. Plesset, Phys. Rev. **46**, 618 (1934).
[45] R. J. Bartlett, Annu. Rev. Phys. Chem. **32**, 359 (1981).
[46] W. J. Hehre, L. Radom, P. v. R. Schleyer, and J. A. Pople, *Ab Initio Molecular Orbital Theory* (Wiley, New York, 1986).
[47] M. J. Frisch, G. W. Trucks, H. B. Schlegel *et al.*, GAUSSIAN 98, Revision A.3, Gaussian, Inc., Pittsburgh, PA, 1998.
[48] P. L. Geissler, T. V. Voorhis, and C. Dellago, Chem. Phys. Lett. **324**, 149 (2000).
[49] P. L. Geissler, C. Dellago, D. Chandler, J. Hutter, and M. Parrinello, Chem. Phys. Lett. **321**, 225 (2000).
[50] S. Yamaguchi, S. Kudoh, Y. Okada, T. Orii, K. Takeuchi, T. Ichikawa, and H. Nakai, J. Phys. Chem. A **107**, 10904 (2003).

Downloaded 11 Aug 2009 to 155.97.13.46. Redistribution subject to AIP license or copyright; see http://jcp.aip.org/jcp/copyright.jsp